



# Structural, magnetic, magnetocaloric and critical exponents of oxide manganite $\text{La}_{0.7}\text{Sr}_{0.3}\text{Mn}_{0.95}\text{Fe}_{0.05}\text{O}_3$

I. Dhahri<sup>1</sup> · M. Ellouze<sup>1</sup> · T. Mnasri<sup>2</sup> · E. K. Hlil<sup>3</sup> · Rajshree B. Jotania<sup>4</sup>

Received: 9 February 2020 / Accepted: 12 June 2020 / Published online: 26 June 2020  
© Springer Science+Business Media, LLC, part of Springer Nature 2020

## Abstract

In this scientific paper, structural, magnetic, magnetocaloric and critical exponent's properties of  $\text{La}_{0.7}\text{Sr}_{0.3}\text{Mn}_{0.95}\text{Fe}_{0.05}\text{O}_3$  compound are briefly reviewed. The sample was synthesized by solid state reaction. X-ray powder diffraction analysis at room temperature showed that our sample is single phase without detection of any impurities. The refinement by the Rietveld method indicate that this compound crystallize in the orthorhombic structure with the space group Pnma. The variation of the magnetization versus temperature found that our perovskite has a single transition from the paramagnetic state (PM) to the ferromagnetic state (FM) with increasing temperature and the obtained Curie temperature is  $T_C = 311$  K. The obtained value of  $|\Delta S_M^{\text{MAX}}|$  is about  $2.3 \text{ J kg}^{-1} \text{ K}^{-1}$  under an applied magnetic field of 5 T. The achieved results show that our compound is a promising candidate for magnetic refrigeration. Also, to discover the nature of the paramagnetic-ferromagnetic phase transition, for the  $\text{La}_{0.7}\text{Sr}_{0.3}\text{Mn}_{0.95}\text{Fe}_{0.05}\text{O}_3$  we made an experimental study on the critical behaviour around the FM-PM transition. The value of the Curie temperature and the critical exponent's  $\beta$ ,  $\gamma$  and  $\delta$  were determined using modified Arrott plots (MAP).

## 1 Introduction

The search for new magnetic materials for high performance magnetic entropy for applications has resulted in exponential growth in both scientific research in this field, and investment in such materials production. In addition, due to their potential applications for devices, colossal magnetoresistance (CMR) and magnetocaloric effect (MCE) in various perovskite oxide manganite's has become a subject of considerable research interest, and the challenge of fully understanding the fundamental nature of the intense interplay between magnetic order, electronic transport, structural distortions and elastic properties in these materials. Manganite's has been created a great deal of interest in the

last century, thanks to their magnetic and electrical properties. For the base compound  $A_{1-x}B_x\text{MnO}_3$  ( $A$  = rare earth like Pr, La, Na... and  $B$  = divalent element like Sr, Ca, Ba...), which belong to perovskite structure, have been study, due to their crucial role in many applications such as magnetocaloric refrigeration [1, 2] and giant magnetoresistance [3]. For Lanthanum based materials and oxides, the substitution of  $\text{La}^{3+}$  ions with alkaline earth metal ions (e.g.  $\text{Sr}^{2+}$ ,  $\text{Ba}^{2+}$ ,  $\text{Ca}^{2+}$ , etc.) is a requirement for a low-cost solutions as they have excellent magnetic properties close to room temperature, in particular Collosal magnetoresistance (CMR), MC effect and semi-metallic properties close to disk heads and magnetic field sensor [4, 5]. Nano-magneto-caloric materials are adapted to practical nanometre-scale magnetic refrigeration equipment. As a result, researches concentrated on working on small magnetic materials (e.g. nanoparticles, thin film, nanowires, multilayer systems, etc.) and new magnetic materials production [6, 8]

The discovery of these physical–chemical properties, this way opens up an area of a fundamental and applied research. The variety of properties makes this type of materials candidate for using in magnetic cooling technology [9, 11]. The magnetism in these materials comes essentially from manganese characterized by a high magnetic moment ( $S = 2$  for  $\text{Mn}^{3+}$  and  $S = 3/2$  for  $\text{Mn}^{4+}$ ). The nature of the paramagnetic-ferromagnetic transition is important to

✉ M. Ellouze  
Mohamed.Ellouze@fss.rnu.tn

<sup>1</sup> Faculty of Sciences of Sfax, LaMMA, Sfax University, B.P. 1171, 3000 Sfax, Tunisia

<sup>2</sup> Research Unit of Physics, Computing and Mathematics, University of Gafsa, 2112 Gafsa, Tunisia

<sup>3</sup> Institut Néel, CNRS - Université Joseph Fourier, BP 166, 38042 Grenoble Cedex9, France

<sup>4</sup> Department of Physics, Electronics and Space Science, University School of Sciences, Gujarat University, Ahmedabad 380 009, India

better understand the metal–insulator transition. In addition, several studies on critical behaviours and the universality class around the Curie temperature have known that critical exponents play important roles in elucidating mechanisms of interactions near  $T_C$  [12, 13].

Furthermore, many other properties have been discovered by doping Mn with a transition metal. The principal character of these compounds is the mixed valence of the manganese ions ( $Mn^{3+}/Mn^{4+}$ ), that is the central reason of ferromagnetic character due to the double exchange between  $Mn^{3+}$  and  $Mn^{4+}$  [14, 16]. Besides all these properties, a lot of work was done about the substitution of the manganese by other 3d metal ions such as iron [17, 19]. Therefore, the substitution of  $Fe^{3+}$  for  $Mn^{3+}$  is not expected to change the tolerance factor, for that reason, the effect of the Jahn–Teller distortion may be neglected. Mössbauer spectroscopy is an effective way to examine octahedral symmetry at the Fe sites [20]. MCE in these oxides is characterized by adiabatic temperature change ( $\Delta T_{ad}$ ) or isothermal magnetic entropy change ( $\Delta S_M$ ), which is a function of both magnetic field and temperature. Partial substitution of Mn by Fe was found to decrease the magnetization and Curie temperature, but the mag-

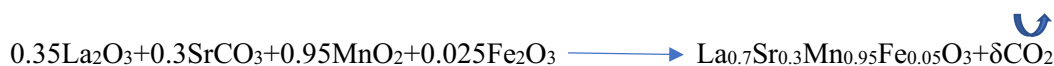
the effect of the crystalline field the orbitals are destabilized. Consequently, degeneration has been lifted. 3d orbitals are divided into sub-levels  $t_{2g}$  and  $e_g$ .

To better illustrate the magnetic properties, in this work, we report on effect of 5% of Fe doping in  $La_{0.7}Sr_{0.3}MnO_3$  on the structural, magnetic, magnetocaloric effect properties and critical exponents. This compound has been synthesized in the literature by several methods of elaboration [26]. The manganite was elaborated with the solid state reaction and characterized by X-ray diffraction (XRD) and magnetization measurements. The magnetocaloric effect was examined as well as the Arrott plot.

## 2 Experimental details

In this work, the sample was elaborated by solid state reaction at higher temperature, using oxides in form of powders. This process is used for the industrial powder production. Nevertheless, this technique may be ineffectual in controlling the grain size and morphology of the powder product. The precursors used are:  $La_2O_3$ ,  $SrCO_3$ ,  $MnO_2$  and  $Fe_2O_3$ .

First, our precursors are weighted in the stoichiometric proportions desired by the reaction equation:



netic entropy shift values remained within the range appropriate for magnetic cooling.

Reviewing previous research, several works centred on materials based on  $La_{1-x}Sr_xMnO_3$  which showed different Curie temperature values [21, 22]. The parent compound  $La_{0.7}Sr_{0.3}MnO_3$  exhibits a Curie temperature about 370 K [23]. In fact, Fe substitution in  $La_{0.7}Sr_{0.3}MnO_3$  deserves precise interest due to magnetic properties of the iron. Leung et al. were among the first to study the effect of iron substitution, they studied the magnetic properties of the compound  $La_{1-x}Pb_xMn_{1-y}Fe_yO_3$ , and deduced the relationship between the antiferromagnetic interactions (AFM)  $Fe^{3+}-O-Fe^{3+}$  and  $Fe^{3+}-O-Mn^{3+}$  and the double exchange ferromagnetic interactions  $Mn^{3+}-O-Mn^{4+}$  [24]. Damay et al. [25] found several orders of decrease in resistivity when applying a magnetic field in the  $Sm_{0.7}Sr_{0.3}Mn_{1-x}Fe_xO_3$  ( $x=0.03$ ) series compared to  $x=0.0$ . The insertion of  $Mn^{3+}$  ( $r_{Mn^{3+}}=0.720 \text{ \AA}$ ) with the ferromagnetic ion  $Fe^{3+}$  ( $r_{Fe^{3+}}=0.785 \text{ \AA}$ ) which have many results such as an increase in lengths of Mn–O, an increase in angles Mn–O–Mn, and as a result a weakening of the ferromagnetic state. The iron atom is placed in the centre of an octahedron, so there is the creation of an electrostatic field whose influence is the division of the levelled. Under

Then, the beginning materials were mixed in order to get a homogeneous mixture. The stoichiometric compound was then placed in alumina crucible and heated to a temperature of 700 °C for 20 h. Subsequently, the obtained powder was pressed into pellets and sintered at 900 °C, 1100 °C, and 1300 °C for 20 h with intermediate regrinding and pelletizing to acquire a better crystal. Finally, these pellets were sintered at 1400 °C for 4 h.

To check the structural and phase purity, we use X-ray powder diffraction using Copper radiation ( $\lambda_1 = 1.54059 \text{ \AA}$  and  $\lambda_2 = 1.52442 \text{ \AA}$ ). The magnetization measurements versus temperature  $M(T)$  in the range 0–450 K, and the isothermal magnetization curves in an applied magnetic field of up to 6 T were obtained using the BS1 magnetometer facility at Louis Neel Grenoble Laboratories. The MEC was estimated from isothermal magnetization measurements versus an applied field up to 5 T.

## 3 Results and discussion

### 3.1 Structural properties

The structural refinement of the diffractogram where performed by the Rietveld method [27] using FullProf code [28]

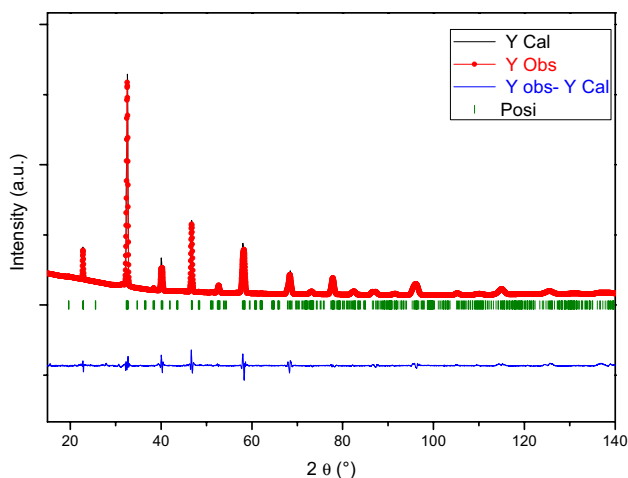


**Fig. 1** XRD patterns for  $\text{La}_{0.7}\text{Sr}_{0.3}\text{Mn}_{0.95}\text{Fe}_{0.05}\text{O}_3$

**Table 1** Refined structural parameters for  $\text{La}_{0.7}\text{Sr}_{0.3}\text{Mn}_{0.95}\text{Fe}_{0.05}\text{O}_3$

	$\text{La}_{0.7}\text{Sr}_{0.3}\text{Mn}_{0.95}\text{Fe}_{0.05}\text{O}_3$	$\text{La}_{0.7}\text{Sr}_{0.3}\text{MnO}_3$ [23]
$a(\text{Å})$	5.4584 <sub>3</sub>	5.4559 <sub>4</sub>
$b(\text{Å})$	7.7454 <sub>1</sub>	7.7368 <sub>6</sub>
$c(\text{Å})$	5.5142 <sub>9</sub>	5.5090 <sub>4</sub>
$V(\text{Å}^3)$	233.13 <sub>5</sub>	232.54 <sub>6</sub>
La/Sr		
X	0.0060 <sub>1</sub>	-0.0081 <sub>7</sub>
Y	0.25	0.25
Z	0.0022 <sub>6</sub>	-0.0004 <sub>9</sub>
Mn/Fe		
X	0.0000	0.0000
Y	0.0000	0.0000
Z	0.5000	0.5000
O <sub>1</sub>		
X	0.4920 <sub>4</sub>	0.5009 <sub>3</sub>
Y	0.25	0.25
Z	0.0173 <sub>2</sub>	0.0216 <sub>3</sub>
O <sub>2</sub>		
X	0.2684 <sub>2</sub>	0.2730 <sub>6</sub>
Y	0.0334 <sub>2</sub>	0.0291 <sub>1</sub>
Z	0.7355 <sub>6</sub>	0.7391 <sub>6</sub>
$\chi^2$	4.84	4.31

The numbers in subscript represent the error bars

(Fig. 1). The structure analysis showed that our compound crystallizes in the orthorhombic system with space group Pnma. Crystal structure parameters and  $\chi^2$  (the reliability factors) are summarized in Table 1. The positions atoms deduced from structural analysis are  $4c(x, 0.25, z)$  for La/Sr,  $4b(0, 0, 0.5)$  for Mn/Fe,  $4c(x, 0.25, z)$  for oxygen ions occupied two different sites, namely O1 at  $4c(x, 0.25, z)$ , and O2 at  $8d(x, y, z)$ . A single phase was observed without any

detectable impurities. It is noted that the lattice parameters and the volume of the unit cell only increased significantly when manganese was substituted by iron. The ionic radius of  $\text{Mn}^{3+}$  (0.645 Å) is equal to that of  $\text{Fe}^{3+}$ [20], consequently, we have noticed that the substitution of manganese by 5% of iron allows a slight increases of the unit cell volume from  $232.55 \text{ Å}^3$  for  $x=0$  to  $233.14 \text{ Å}^3$  for  $x=0.05$  as well as for unit cells parameters. Our results are agreed to those obtained by Yanchevski et al. [29] and Huang et al. [30].

The tolerance factor of Goldschmidt [31] was calculated using:

$$t = \frac{r_A + r_O}{\sqrt{2}(r_B + r_O)} \tag{1}$$

with:  $r_A$  is the radius of the cation occupying site A,  $r_B$  is the radius of the cation occupying site B and  $r_O$  is the oxygen radius.

According to the electrical neutrality law of our compound:

$$0.7\text{La}^{3+} + 0.3\text{Sr}^{2+} + 0.65\text{Mn}^{3+} + 0.3\text{Mn}^{4+} + 0.05\text{Fe}^{3+} + \text{O}_3^{2-}$$

so:

$$r_A = 0.7r_{\text{La}^{3+}} + 0.3r_{\text{Sr}^{2+}}$$

$$r_B = 0.65r_{\text{Mn}^{3+}} + 0.3r_{\text{Mn}^{4+}} + 0.05r_{\text{Fe}^{3+}}$$

Accordingly, the calculation of the tolerance factor ( $t=0.92$ ) shows that the structure of our sample is orthorhombic, what is confirmed with Rietveld refinement.

The average crystallite size was estimated from X-ray diffraction using Debye–Scherrer formula [32]:

$$D = \frac{K\lambda}{\beta \cos(\theta)} \tag{2}$$

where  $K$ ,  $\lambda$ ,  $\beta$ , and  $\theta$  are the grain shape factor, the X-ray wavelength, the full width at half maximum (FWHM) of the diffraction peak and the Bragg diffraction angle, respectively. The value of the effective crystallite size is 24 nm.

To draw the unit cell, we used “Diamond” program (Fig. 2), in order to determine distances Mn–O<sub>1</sub> and Mn–O<sub>2</sub> and the inter-atomic angles Mn–O–Mn. The results obtained are listed in Table 2.

### 3.2 Magnetic properties

Figure 3 indicates the magnetization of  $\text{La}_{0.7}\text{Sr}_{0.3}\text{Mn}_{0.95}\text{Fe}_{0.05}\text{O}_3$  as a function of temperature for an applied field of 0.05 T. The compound reveals a transition from a ferromagnetic state at low temperature to a paramagnetic state followed by a rapid increase of magnetization around the Curie Temperature ( $T_C$ ). The value of this

**Fig. 2** Crystal structure of  $\text{La}_{0.7}\text{Sr}_{0.3}\text{Mn}_{0.95}\text{Fe}_{0.05}\text{O}_3$

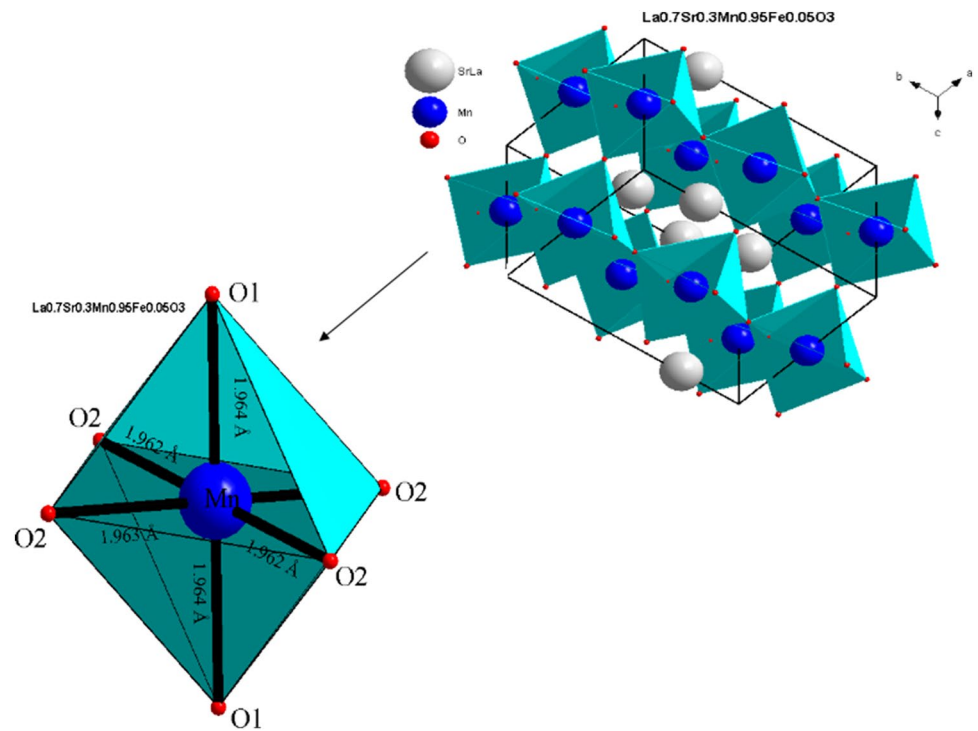


**Table 2** Interatomic distances Mn–O and angles Mn–O–Mn for  $\text{La}_{0.7}\text{Sr}_{0.3}\text{Mn}_{0.95}\text{Fe}_{0.05}\text{O}_3$

Distances (Å)	$\text{La}_{0.7}\text{Sr}_{0.3}\text{Mn}_{0.95}\text{Fe}_{0.05}\text{O}_3$
Mn (Fe)–O <sub>1</sub>	1.964
Mn (Fe)–O <sub>2</sub>	1.962
Angles (°)	
Mn (Fe)–O <sub>1</sub> –Mn (Fe)	176.90
Mn (Fe)–O <sub>2</sub> –Mn (Fe)	171.48

temperature is determined at the inflection point of  $M(T)$ , obtained from the minimum of  $dM/dT$ , and it is found equal to 311 K, which is low than that reported by Brik et al. [33],  $T_C = 343$  K. This difference between the two values is probably due to the experimental conditions: elaboration method and temperatures.

Moreover, some studies on the magnetic measurements indicates that the Curie temperature decrease with increasing the Fe content [33–35]. The observed decrease in magnetization and  $T_C$  with doping iron could be correlated with the fact that  $\text{Fe}^{3+}$  ions do not engage in the ferromagnetic double exchange (DE) interaction with  $\text{Mn}^{3+}$  ions,

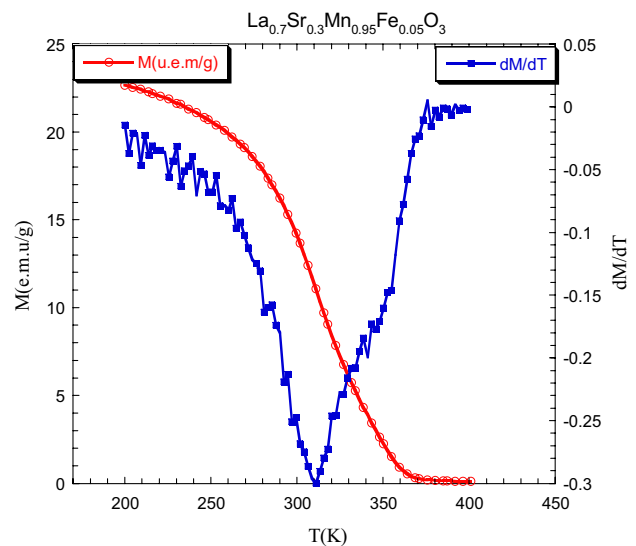


**Fig. 3** Magnetization versus temperature under an applied field of 0.05 T and The  $dM/dT$  curve

but instead promote the antiferromagnetic interactions  $\text{Fe}^{3+}\text{--O--Mn}^{3+}$ ,  $\text{Mn}^{4+}\text{--O--Fe}^{3+}$  and  $\text{Fe}^{3+}\text{--O--Fe}^{3+}$  super-exchange (SE) interactions [36].

We plotted, (Fig. 4), the inverse of the susceptibility in the paramagnetic state, deduced from the  $M(T)$  curves at an applied field of 0.05 T. The Weiss temperature and the

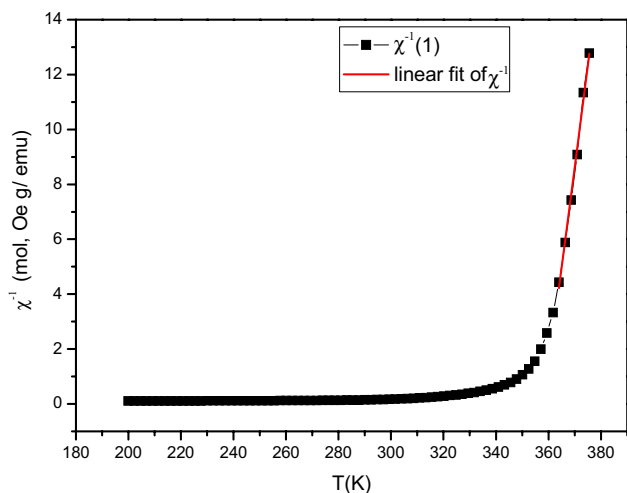


**Fig. 4** The inverse of susceptibility of the sample  $\text{La}_{0.7}\text{Sr}_{0.3}\text{Mn}_{0.95}\text{Fe}_{0.05}\text{O}_3$

**Table 3** Magnetic data of  $\text{La}_{0.7}\text{Sr}_{0.3}\text{Mn}_{0.95}\text{Fe}_{0.05}\text{O}_3$ : The Curie temperature  $T_C$ , the Curie–Weiss temperature, the experimental effective paramagnetic moment and theoretical effective paramagnetic moment

Compound	$T_C$ (K)	$\Theta_w$ (K)	$\mu_{\text{eff}}(\text{exp})$ ( $\mu_B$ )	$\mu_{\text{eff}}(\text{cal.})$ ( $\mu_B$ )
$\text{La}_{0.7}\text{Sr}_{0.3}\text{Mn}_{0.95}\text{Fe}_{0.05}\text{O}_3$	311	357	3.28	4.28

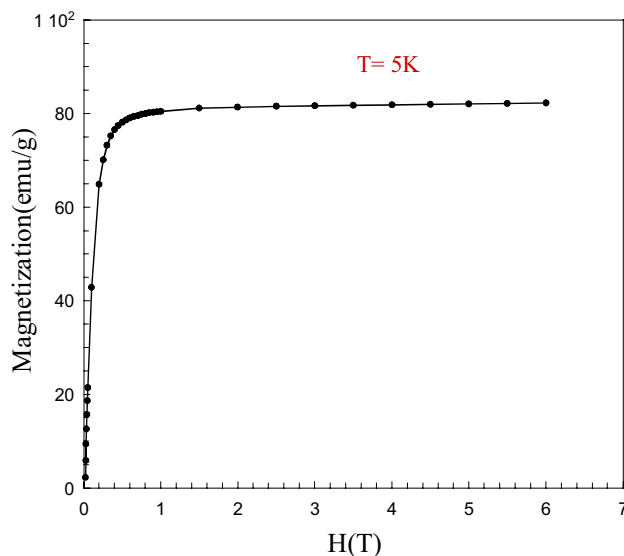
Curie constant were so determined using the Curie–Weiss formula:

$$\chi = \frac{C}{T - \theta_w} \tag{3}$$

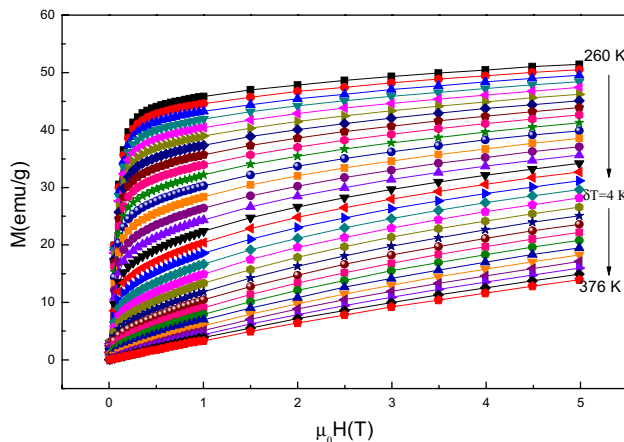
where  $C$  is the Curie constant and  $\theta_w$  is the Weiss temperature.

Figure 4 shows a deviation of  $\chi^{-1}(T)$  from the linearity around  $T_C$ . We obtained the estimated values of the Curie constant and the paramagnetic Curie temperature  $\theta_w$ . The experimental effective magnetic moment  $\mu_{\text{eff}}(\text{exp.})$  were deduced from the estimated Curie constant and compared with the theoretical value  $\mu_{\text{eff}}(\text{cal.})$  (Table 3). The difference between the experimental and calculated values is due to the presence of ferromagnetic clusters in the paramagnetic state [37].

The magnetization curve  $M(H)$  at  $T = 5$  K is shown in Fig. 5. Our sample is obviously ferromagnetic at this temperature and almost saturated at an applied field of 6 T. The saturation magnetization for our sample is about  $3.3 \mu_B$ . Important the magnetic properties of the ordering of cations in the A-sublattice of perovskite can be explained by chemical phases. The separation takes into account the compression effect, which is the result of the action of chemicals and external pressure (surface tension) [38].



**Fig. 5** Magnetization versus an applied field at 5 K



**Fig. 6** Isothermal magnetization curves measured at different temperatures

### 3.3 Magnetocaloric properties

In Fig. 6, we plotted the evolution of magnetization versus the applied magnetic field at different temperatures [260, 376 K] with a step of 4 K around Curie temperature. This figure shows an increase of magnetization when the applied magnetic field is less than 0.5 T and saturates above 1 T. The saturation magnetization increases when the temperature decreases, which confirms the ferromagnetic behaviour at low temperatures. This compartment is typical of a soft magnetic material.

The curves for  $\text{La}_{0.7}\text{Sr}_{0.3}\text{Mn}_{0.95}\text{Fe}_{0.05}\text{O}_3$  continued to rise and did not saturate even at 5 T. In order to understand the nature of transition we plotted Arrott curves  $M^2$  versus

$\left(\frac{\mu_{0H}}{M}\right)$ . The plots exhibited a positive slope around  $T_C$  which confirms that our sample exhibit second order ferromagnetic to paramagnetic phase transition [39–46].

To investigate the magnetocaloric properties, the magnetic entropy change (MCE,  $\Delta S_M$ ) was calculated. The magnetic entropy change,  $(-\Delta S_M)$ , caused by the increase in the magnetic field was determined using the following equation according to the classical thermodynamic theory based on the relation of Maxwell [47]:

$$\Delta S_M(T)_{\Delta H} = \int_{H_1}^{H_2} \left( \frac{\partial M(T, H)}{\partial T} \right)_H dH \quad (4)$$

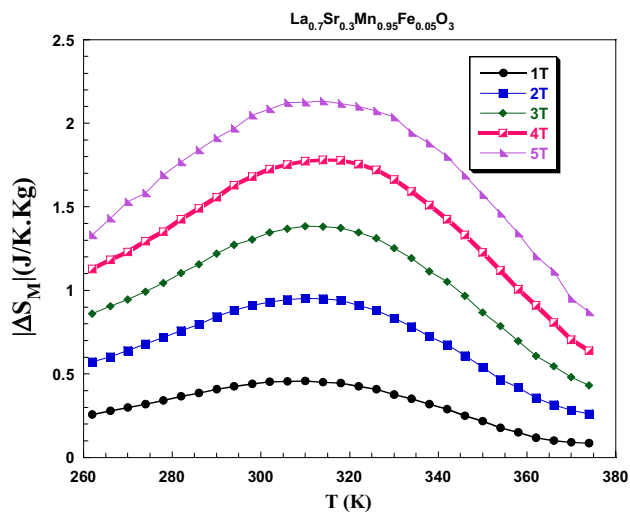


**Fig. 7** Temperature dependence of magnetic entropy change for  $\text{La}_{0.7}\text{Sr}_{0.3}\text{Mn}_{0.95}\text{Fe}_{0.05}\text{O}_3$

**Table 4** Maximum entropy change  $|\Delta S_M^{\text{MAX}}|$ , RCP values and magnetic field change for  $\text{La}_{0.7}\text{Sr}_{0.3}\text{Mn}_{0.95}\text{Fe}_{0.05}\text{O}_3$  in comparison with the literature

Compounds	$ \Delta S_M^{\text{MAX}} $ (J Kg <sup>-1</sup> K <sup>-1</sup> )	RCP (J Kg <sup>-1</sup> )	$\mu_0 H$ (T)	Refs
$\text{La}_{0.7}\text{Sr}_{0.3}\text{MnO}_3$	1.10	49	2	[23]
$\text{La}_{0.7}\text{Sr}_{0.3}\text{MnO}_3$	1.27	29	2	[34]
$\text{La}_{0.7}\text{Sr}_{0.3}\text{Mn}_{0.95}\text{Fe}_{0.05}\text{O}_3$	2.13	127.9	5	This work
$\text{La}_{0.7}\text{Sr}_{0.3}\text{Mn}_{0.95}\text{Fe}_{0.05}\text{O}_3$	2.4	83	2	[33]
$\text{La}_{0.7}\text{Sr}_{0.3}\text{Mn}_{0.93}\text{Fe}_{0.07}\text{O}_3$	0.95	49.46	2	[33]
$\text{La}_{0.7}\text{Sr}_{0.3}\text{Mn}_{0.85}\text{Fe}_{0.15}\text{O}_3$	1.4	97	2	[33]
$\text{La}_{0.7}\text{Sr}_{0.3}\text{Mn}_{0.8}\text{Fe}_{0.2}\text{O}_3$	0.6	90	2	[33]
$\text{La}_{0.7}\text{Sr}_{0.3}\text{Mn}_{0.95}\text{Ti}_{0.05}\text{O}_3$	2.2	90	2	[40]
$\text{La}_{0.7}\text{Sr}_{0.3}\text{Mn}_{0.95}\text{Al}_{0.05}\text{O}_3$	1.4	100	2	[40]
$\text{La}_{0.67}\text{Ba}_{0.22}\text{Sr}_{0.11}\text{Mn}_{0.9}\text{Fe}_{0.1}\text{O}_3$	2.26	153	5	[45]
$\text{La}_{0.67}\text{Ba}_{0.22}\text{Sr}_{0.11}\text{Mn}_{0.8}\text{Fe}_{0.2}\text{O}_3$	1.03	91	5	[45]
$\text{La}_{0.65}\text{Dy}_{0.05}\text{Sr}_{0.3}\text{Mn}_{0.95}\text{Ti}_{0.05}\text{O}_3$	1.79	239	5	[45]
Gd	9.5	410	5	[45]

The numerical integration of the latter formula at different field and temperature conditions gives the values of  $\Delta S_M$ :

$$\Delta S_M = \sum_i \frac{M_{i+1} - M_i}{T_i - T_{i+1}} \Delta H_i \quad (5)$$

where  $M_i$  and  $M_{i+1}$  are experimental values of magnetization at  $T_i$  and  $T_{i+1}$  temperature, respectively, under an applied field  $H_i$ . Figure 7 illustrates the magnetic entropy change  $|\Delta S_M|$  versus temperature at different applied magnetic field from 1 to 5 T. Predictably, the magnetic entropy change increased with the magnetic field applied, and reaches the maximum value around  $T_C$ . The maximum of entropy changes from  $0.46 \text{ J Kg}^{-1} \text{ K}^{-1}$  at an applied field of 1 T to  $2.13 \text{ J Kg}^{-1} \text{ K}^{-1}$  at an applied field of 5 T. The small value of magnetic entropy change can be related to second order magnetic phase transition. As a rule, materials with first order transitions typically exhibit a much greater magnetocaloric effect than those with second order transitions.

Nevertheless, the value of the device studied stems from the ability to adjust its properties and check the structural factors, as well as the facility to synthesize these materials with good chemical stability.

In Table 4, the MCE values obtained in comparison with some others reported in the literature were listed. To calculate the relative cooling power (RCP) the following formula was adopted [47, 48]:

$$\text{RCP} = \left| \Delta S_M^{\text{MAX}} \right| \times \delta T_{\text{FWHW}} \quad (6)$$

$\delta T_{\text{FWHW}}$  is the full width at half maximum of the magnetic entropy and  $|\Delta S_M^{\text{MAX}}|$  is the maximum entropy changes. While iron doping reduces  $T_C$  and  $|\Delta S_M^{\text{MAX}}|$  relatively, the observed properties of the investigated method are promising and open the way for investigations of materials that are useful for magnetic cooling (Fig. 8)..

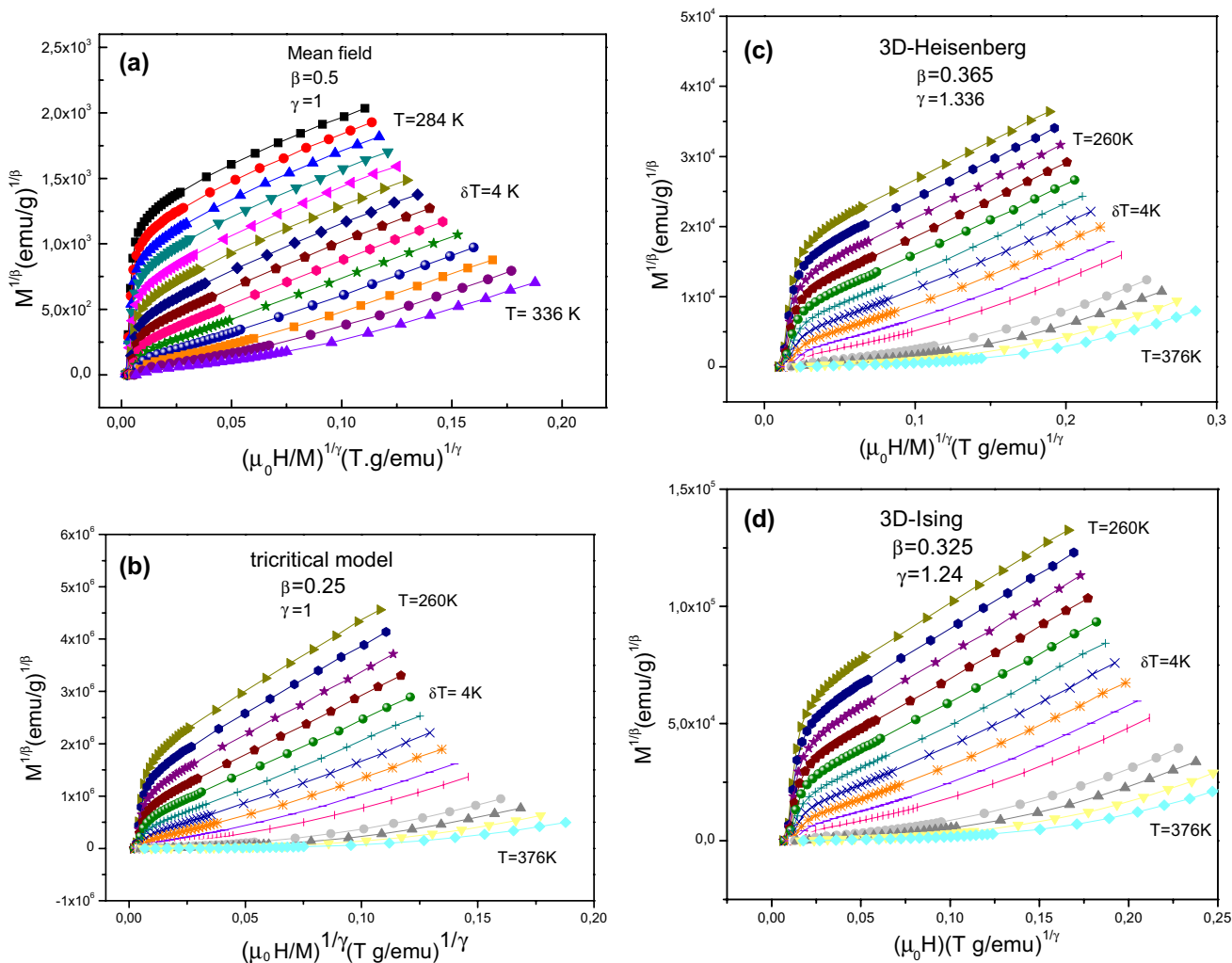


**Fig. 8** **a** Arrott plot curves  $M^2$  versus  $\mu_0 H/M$  for the mean field model, **b** Arrott plots for the tricritical model, **c** Arrott curves for the 3D-Heisenberg model, and **d** Arrott curves for the 3D-Ising model

### 3.4 Critical behaviour

To investigate the critical behaviour of manganese oxide around the FM-PM transition second order magnetic phase transition we used different techniques given a wide range critical exponents:  $\alpha$  (associated to the critical magnetization at Curie temperature),  $\beta$  (associated to the spontaneous magnetization), and  $\delta$  (associated to initial susceptibility) [49–51]. Firstly, these critical exponents defined to apply in the DE model for the long-range mean field theory [11, 52, 53]. Furthermore, the interpretation of some important experimental results on critical exponents and the universality of manganese’s is still controversial [11, 49–55]. In this work we study the critical behaviour of the sample  $\text{La}_{0.7}\text{Sr}_{0.3}\text{Mn}_{0.95}\text{Fe}_{0.05}\text{O}_3$  oxide using modified Arrott-Plots (MAP). In addition, according to Banerjee, the positive slope indicates a second order phase transition [56]. Arrott and Noakes proposed a strong tool, the

MAPs, to use the following empirical relation to evaluate magnetic data [39]:

$$\left(\frac{H}{M}\right)^{\frac{1}{\gamma}} = \frac{T - T_C}{T_1} + \left(\frac{M}{M_1}\right)^{\frac{1}{\beta}} \tag{7}$$

where  $T_1$  and  $M_1$  are constants characterizing the compound.

Then a linear relation between  $M^{\frac{1}{\beta}}$  and can be sought by proper choice of  $\beta$  and  $\gamma$ . Thus by choosing the critical parameters of a given universality class, a linear relation means that the compound belongs to that class.

Figure 8a-d show the variation of modified Arrott plots  $M^{\frac{1}{\beta}}$  versus  $\left(\frac{H}{M}\right)^{\frac{1}{\gamma}}$  for different models: mean field theory ( $\beta = 0.5$ ;  $\gamma = 1$ ); the 3D-Ising model ( $\beta = 0.325$ ;  $\gamma = 1.241$ ); the tricritical mean-field model ( $\beta = 0.25$ ;  $\gamma = 1$ ), and the 3D-Heisenberg model ( $\beta = 0.365$ ;  $\gamma = 1.336$ ).

The scaling hypothesis offers a basis for characterizing a second order phase transition by the values of the critical exponent  $\beta$ ,  $\gamma$  and  $\delta$  for spontaneous magnetization, initial magnetic susceptibility and critical isothermal magnetization, respectively [56]. The magnetic parameters are given in relation to these exponents by the following relationships:

- Spontaneous magnetization under  $T_C$  at the zero-applied field limit is given by Eq. 7:

$$M_S(T) = M_0(-\varepsilon)^\beta \quad T < T_C \quad (8)$$

- The initial susceptibility is given over above  $T_C$  by Eq. 8:

$$\chi_0^{-1}(T) = \left(\frac{h_0}{M_0}\right) \varepsilon^\gamma \quad T > T_C \quad (9)$$

- At  $T_C$ , magnetization  $M$  is based on magnetic field  $H$  using Eq. 9:

$$M = D_0 H^{\frac{1}{\alpha}}; \quad T = T_C \quad (10)$$

Where  $\varepsilon$  is the reduced temperature  $\varepsilon = (T - T_C)/T_C$ ,  $M_0$ ,  $h_0$  and  $D$  are critical amplitudes.

Using the adjust of  $M^{\frac{1}{\beta}}$  versus  $\left(\frac{\mu_0 H}{M}\right)$  near  $T_C$ , we can deduce the values of  $\beta$  and  $\gamma$ . The obtained curves are parallel to each other in high field region, then that at  $T_C$  we have straight line and the  $\alpha$  value are directly determined by the linear fit of magnetization. In order to deduce  $M_S(T)$  (Spontaneous magnetization) and  $\chi_0^{-1}(T)$  (inverse initial susceptibility), we investigate the extrapolation of linear part of MAPs in range of the high magnetic field in intersect with  $(H/M)^{1/\gamma}$  and  $M^{1/\beta}$  (Fig. 9). On the other way they can be calculated using the Widom relation with  $\beta$  and  $\gamma$  [56]:

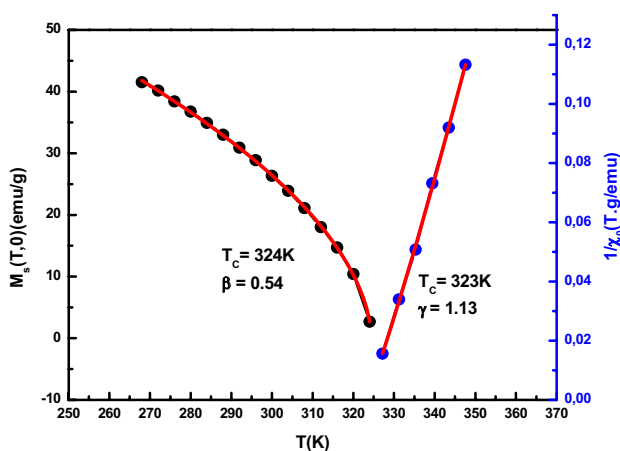


**Fig. 9** The fits of spontaneous magnetization and initial inverse of susceptibility versus temperature

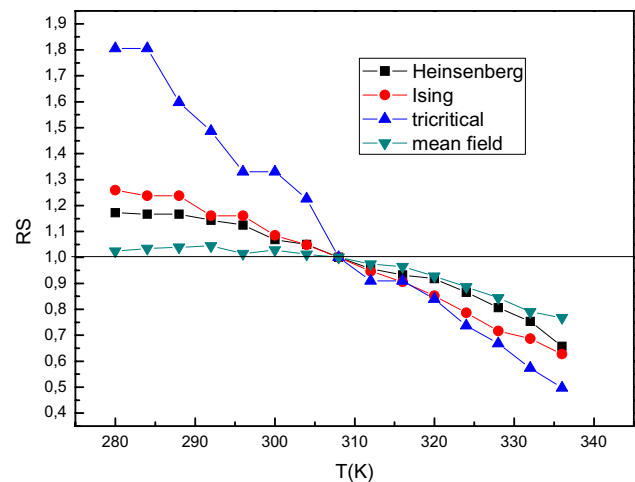


**Fig. 10** Relative slope RS versus temperature

$$\alpha = 1 + \frac{\gamma}{\beta} \quad (11)$$

The obtained values using MAP are:  $\beta = 0.54$ ;  $\gamma = 1.13$ ;  $\alpha = 3.07$ . The results show that the critical exponents are consistent with the mean field model which is confirmed with the relative slope  $RS = S(T)/S(T_C)$  in the high field region around  $T_C$ , Fig. 10.

## 4 Conclusion

In summary, we have elaborated and investigated structural, magnetic, magnetocaloric and critical exponents of the manganite oxide  $\text{La}_{0.7}\text{Sr}_{0.3}\text{Mn}_{0.95}\text{Fe}_{0.05}\text{O}_3$ . The sample was elaborated by solid state reaction. Using Rietveld refinement, the compound crystallized in the orthorhombic structure with Pnma space group. Magnetic measurement shows that the sample exhibits a transition from paramagnetic to ferromagnetic state with decreasing temperature. The substitution of manganese with 5% of iron does not cause a structural transition, but modify the crystallographic parameters, and decreases the  $T_C$  value. The magnetocaloric study indicates that the  $|\Delta S_M^{\text{MAX}}|$  reaches its maximum value at an applied magnetic field 5 T near  $T_C$ . The RCP value of doped compound was found to be  $127.9 \text{ J Kg}^{-1}$  at  $\Delta H = 5 \text{ T}$ , which is suitable for potential application in magnetic refrigeration and heat storage near  $T_C$ ). Finally, the critical exponents  $\alpha$ ,  $\beta$ , and  $\gamma$  were evaluated from modified Arrott plots. They are consistent with those of mean field model.



## References

- S. Othmani, M. Bejar, E. Dhahri, E.K. Hlil, J. Alloys Compd. **475**, 46 (2009)
- S. Kossi, S. Ghodhbane, S. Mnefqi, J. Dhahri, E.K. Hlil, J. Magn. Magn. Mater. **395**, 134–142 (2015)
- A. Dhahri, M. Jemmali, E. Dhahri, E.K. Hlil, Dalton Trans. **44**(12), 5620–5627 (2015)
- Y. Sun, W. Tong, N. Liu, Y. Zhang, J. Magn. Magn. Mater. **238**, 25–28 (2002)
- M. Pekala, V. Drozd, J. Alloys Compd. **456**, 30–33 (2008)
- N.T.M. Duc et al., J. Alloys Compd. **807**, 151694 (2019)
- J.H. Belo, A.L. Pires, J.P. Araújo, A.M. Pereira, J. Mater. Res. **34**, 134–157 (2019)
- S.K. Giri et al., J. Phys. D. **52**, 165302 (2019)
- M.H. Phan, S.C. Yu, J. Magn. Magn. Mater. **308**, 325 (2007)
- A.M. Aliev, A.G. Gamzatov, K.I. Kamilov, A.R. Kaul, N.A. Babushkina, Appl. Phys. Lett. **101**, 172401 (2012)
- C. Martin, A. Maignan, M. Hervieu, B. Raveau, Phys. Rev. B **60**, 12191 (1999)
- M. Triki, E. Dhahri, E.K. Hlil, J. Solid State Chem. **201**, 63–67 (2013)
- S. Ghodhbane, E. Tka, J. Dhahri, E.K. Hlil, J. Alloys Compd. **600**, 172–177 (2014)
- A. Moreo, S. Yunoki, E. Dagotto, Science **283**, 2034 (1999)
- F. Ben Jemaa, S. Mahmood, M. Ellouze, E.K. Hlil, F. Halouani, J. Mater. Sci. **50**, 620 (2015)
- F. Ben Jemaa, S. Mahmood, M. Ellouze, E.K. Hlil, E. Halouani, Ceram. Int. **41**, 8291 (2015)
- S.C. Hong, S.J. Kim, E.J. Hahn, S.I. Park, C.S. Kim, IEEE Trans. Magn. **45**, 6 (2009)
- E.K. Abdel-Khalek, W.M. El-Meligy, E.A. Mohamed, T.Z. Amer, H.A. Sallam, J. Phys. Condens. Matter. **21**, 026003 (2009)
- H.Y. Hwang, S.-W. Cheong, P.G. Radaelli, M. Marezio, B. Batlogg, Phys. Rev. Lett. **914–917**, 75 (1995)
- R.D. Shannon, Revised effective ionic radii and systematic studies of interatomic distances in halides and chalcogenides. Acta Crystallogr. **32**, 751–767 (1976)
- S.V. Trukhanov, Peculiarities of the magnetic state in the system  $\text{La}_{0.70}\text{Sr}_{0.30}\text{MnO}_{3-\gamma}$  ( $0 \leq \gamma \leq 0.25$ ). J. Exp. Theor. Phys. **100**(1), 95–105 (2005)
- S.V. Trukhanov, A.V. Trukhanov, A.N. Vasilev, A. Maignan, H. Szymczak, Critical behavior of  $\text{La}_{0.825}\text{Sr}_{0.175}\text{MnO}_{2.912}$  anion-deficient manganite in the magnetic phase transition region. JETP Lett. **85**(10), 507–512 (2007)
- R. Cherif, S. Zouari, M. Ellouze, E.K. Hlil, F. Elhalouani, Phys. J. Plus **129**, 83 (2014)
- L.K. Leung, A.H. Morrish, B.J. Evans, Phys. Rev. B **13**, 4069 (1976)
- F. Damay, A. Maignan, N. Nguyen, B. Raveau, J. Solid State Chem. **124**, 385 (1996)
- N. Kemik, Y. Takamura, A. Navrotsky, J. Solid State Chem. **184**, 2118–2123 (2011)
- H.M. Rietveld, Appl. Cryst. **2**, 65 (1967)
- J. Rodriguez-Cararjal, Full Prof (U B Saclay, France, 1998)
- O.Z. Yanchevski, O.I.V. Yunov, A.G. Belovs, Fiz. Nizk. Temp. **32**, 184 (2006)
- Q. Huang, Z.W. Li, J. Liand, C.K. Ong, J. Phys. Condens. Matter. **13**, 4033 (2001)
- M.I. Mendelson, J. Am. Ceram. Soc. **52**, 443 (1969)
- A. Guinier, in: X. Dunod (Ed.), Théorie et technique de la Radiocristallographie, (1964), Dunod: Paris, p. 482.
- S.K. Barik, C. Krishnamoorthi, R. Mahendiran, J. Magn. Magn. Mater. **323**, 1015 (2011)
- N. Kallel, S. Kallel, A. Hagaza, M. Oumezzine, Phys. B **404**, 285 (2009)
- S.M. Yusuf, M. Sahana, M.S. Hegde, K. Dörr, K.-H. Müller, Phys. Rev. B. **62**, 1118 (2000)
- R. Masrour, A. Jabar, H. Khelif, F. Ben Jemaa, M. Ellouze, E.K. Hlil, Solid State Commun. **268**, 64–69 (2017)
- B. Martinez, V. Laukhin, J. Fontcuberta, L. Pinsard, A. Revcolevschi, Phys. Rev. B **66**, 054436 (2002)
- S.V. Trukhanov, V.A. Khomchenko, L.S. Lobanovski, M.V. Bushinsky, D.V. Karpinsky, V.V. Fedotova, A. Adair, Crystal structure and magnetic properties of Ba-ordered manganites  $\text{Ln}_{0.70}\text{Ba}_{0.30}\text{MnO}_{3-\delta}$  ( $\text{Ln} = \text{Pr}, \text{Nd}$ ). J. Exp. Theor. Phys. **103**(3), 398–410 (2006)
- A. Arrott, J.E. Noakes, Phys. Rev. Lett. **19**, 786–789 (1967)
- D.N.H. Nam, N.V. Dai, L.V. Hong, N.X. Phuc, S.C. Yu, M. Tachibana, E. Takayama-Muromachi, J. Appl. Phys. **103**, 043905 (2008)
- M. Baazaoui, S. Zemni, M. Boudard, H. Rahmouni, A. Gasmi, A. Selmi, M. Oumezzin, Int. J. Nanoelectron. Mater. **3**, 23–26 (2010)
- S.M. Yusuf, J.M. De Teresa, P.A. Algarabel, J. Blasco, M.R. Ibarra, A. Kumar, C. Ritter, Phys. B **401**, 385–386 (2006)
- R.D. McMichael, J.J. Ritter, R.D. Shull, Enhanced magnetocaloric effect in  $\text{Gd}_3\text{Ga}_{5-x}\text{Fe}_x\text{O}_{12}$ . J. Appl. Phys. **73**, 6946 (1993)
- S. Ghodhbane, A. Dhahri, N. Dhahri, E.K. Hlil, J. Dhahri, M. Alhabrabi, M. Zaidi, J. Alloys Compd. **580**, 558–656 (2013)
- F. Ben Jemaa, S. Mahmood, M. Ellouze, E.K. Hlil, F. Halouani, I. Bsoul, M. Awawdeh, Structural, magnetic and magnetocaloric properties of  $\text{La}_{0.67}\text{Ba}_{0.22}\text{Sr}_{0.11}\text{Mn}_{1-x}\text{Fe}_x\text{O}_3$  nanopowders. Solid State Sci. **37**, 121–130 (2014)
- R. Felhi, H. Omrani, M. Koubaa, W. Cheikhrouhou-Koubaa, A. Cheikhrouhou, J. Mater. Sci. **30**, 12426–12436 (2019)
- R.D. Mc Michael, J.J. Ritter, R.D. Shull, J. Appl. Phys. **73**, 6946 (1993)
- S. Tapas, I. Das, S. Banerjee, Phys. Lett. **91**, 082511 (2007)
- K. Ghosh, C.J. Lobb, R.L. Greene, S.G. Karabashev, D.A. Shulyatev, A.A. Arsenov, Y. Mukovskii, Phys. Rev. Lett. **81**, 4740–4743 (1998)
- Y. Motome, N. Furukawa, J. Phys. Soc. Jpn. **70**, 1487–1490 (2001)
- P. Zhang, P. Lampen, T.L. Phan, S.C. Yu, T.D. Thanh, N.H. Dan, V.D. Lam, H. Srikanth, M.H. Phan, J. Magn. Magn. Mater. **348**, 146–153 (2013)
- P.W. Anderson, H. Hasegawa, Phys. Rev. **100**, 575–681 (1955)
- H.E. Stanley, Introduction to Phase Transitions and Critical Phenomena (Oxford University Press, London, 1971)
- J.M.D. Coey, M. Viret, S. Von Molnar, Adv. Phys. **48**, 167–293 (1999)
- N. Moutis, I. Panagiotopoulos, M. Pissas, D. Niarxhos, Phys. Rev. B **59**, 1129–1133 (1999)
- B.K. Banerjee, Phys. Lett. **12**, 16–17 (1964)

**Publisher's Note** Springer Nature remains neutral with regard to jurisdictional claims in published maps and institutional affiliations.